

The Bandwidth of Transient Yaw Effects on Vehicle Aerodynamics

2011-01-0160

Published
04/12/2011

Oliver Mankowski and David Sims-Williams

Robert Dominy
Durham Univ

Bradley Duncan and Joaquin Gargoloff
Exa Corporation

Copyright © 2011 SAE International

doi:[10.4271/2011-01-0160](https://doi.org/10.4271/2011-01-0160)

ABSTRACT

A vehicle on the road encounters an unsteady flow due to turbulence in the natural wind, the unsteady wakes from other vehicles and as a result of traversing through the stationary wakes of road side obstacles. There is increasing concern about potential differences in aerodynamic behaviour measured in steady flow wind tunnel conditions and that which occurs for vehicles on the road. It is possible to introduce turbulence into the wind tunnel environment (e.g. by developing active turbulence generators) but on-road turbulence is wide ranging in terms of both its intensity and frequency and it would be beneficial to better understand what aspects of the turbulence are of greatest importance to the aerodynamic performance of vehicles.

There has been significant recent work on the characterisation of turbulent airflow relevant to road vehicles. The simulation of this time-varying airflow is now becoming possible in wind tunnels and in CFD. Less is known about the range of turbulence length scales and intensities that are significant to the performance of vehicles. It is only necessary to simulate (experimentally or computationally) the Venn intersection of the range of conditions experienced and the range that are important to the vehicle's performance.

The focus of this work is on transient yaw fluctuations. Time-resolved simulations of simple two dimensional parametric geometries subjected to yaw transients at a range of different time scales were conducted using Exa Powerflow. The effects

of model geometry, Reynolds number yaw fluctuation amplitude and superposition were investigated.

It was found that, in general, the flow could be treated as quasi-steady for reduced frequencies below 0.3 (based on model length and freestream velocity), which is consistent with theory. The most significant changes were observed in a critical reduced frequency range between $\omega_R = 0.3$ and $\omega_R = 1.5$ (scales of 4-20 vehicle lengths, or periods of 0.6 to 3s for a vehicle at 30 m/s). Higher frequencies will have significant effects, but these were observed to show little sensitivity to frequency above the critical range. Small physical features on real vehicles will add importance to smaller, but not larger, scales.

The dynamic effects were largely independent of Reynolds number, including for near-inviscid conditions, indicating that the sources of the non-quasi-steady response were not viscous in origin. Increasing yaw amplitude or combining multiple frequency components did not have a summative impact suggesting that it may not be possible to describe vehicle response to transient conditions using linear concepts such as transfer or admittance functions.

INTRODUCTION

There has been significant recent work on the characterisation of ground level turbulent airflow relevant to road vehicles (e.g.: as reviewed by [1], [2], [3]). The simulation of this time-varying airflow is now becoming possible in wind tunnels and in CFD (e.g.: [4], [5], [6], [7]). A study is

presented here using CFD on an idealised bluff body in order to develop our fundamental understanding of the turbulent scales of importance, specifically assessing the performance impact of varying harmonic and gust like flows over an idealised body. The geometry used has been primarily based up Docton [8] and Ryan [9] and secondarily from Sims-Williams [10] with the gust profile from Ryan [9]. A variety of transient yaw conditions are simulated to assess their impact on the lateral and drag mean and standard deviation. Of particular interest is assessing the critical range of frequencies (scales) in the onset airflow of importance in terms of the body's aerodynamic response. It is intended that the result of this paper will be of value in the development and operation of turbulence generation systems. The focus is on yaw angle variation as these are, arguably, the most important on road. This works ties in closely with that of Gaylard et al [7] and Thiessen [11]. A direct outcome will be to determine the quasi-steady reduced frequency limit of 0.1 to 1.0 as discussed by He [12] and to further define the significant inlet flow frequency range as proposed by Wordley [13]. Reduced frequency is defined as:

$$\omega_R = \frac{2\pi L}{U} \quad (1)$$

Where L is a characteristic dimension (vehicle length is used here) and U is resultant velocity, though here evaluated as the axial (30ms^{-1}) velocity.

A key focus in vehicle aerodynamic research is determining the frequency range that is most significant to the drag force and stability of vehicles. Wordley [13] was successful at defining the range of frequencies and intensities that characterise ground-level airflow, with a view to guiding the wind tunnel simulation of turbulent conditions for road vehicles. Wordley [13] recognised that generating the full range of conditions experienced by a vehicle on road is problematic and that it would be attractive to only simulate a subset of the full range. It is feasible, that from the range of turbulence experienced by vehicles, that the range of turbulence length scales and intensities that are significant to the performance of the vehicle will be smaller, and as such that the specification for turbulence generation systems could be subsequently narrowed. Wordley [13] suggested that length scales from 0.5 to 15m are key, though recent work by Thiessen [11] has suggested that the relevant upper limit could be as high as 30-90m. Determination of the relevant range would assist the development and operation of such turbulence generation systems. The development of systems to reproduce the full range of relevant length scales is as yet unsolved and inevitably intricate. The simulation of length scales down to 3m is achievable with lift devices [14] and scales below 0.5m can be simulated with passive devices [15], [16] but it is the intermediate scales that provide the greatest challenges [17].

It is expected, as proposed by He [12] and Sims-Williams [3], that the effect of inlet turbulence on vehicle drag and stability will be curtailed by the quasi-steady limit, which this paper will define for a variety of inlet and geometry configurations. The use of idealized models, such as by Ryan [9] and Docton [8], allows a wide range of frequencies to be analysed with regard to the effect of delayed or encouraged separation and other consequential flow features that are apparent with simple geometries. Finally, the ability to assess a range of factors (i.e. corner radii, width, viscosity) in numerical simulations will focus and encourage future simulation analysis.

APPROACH

The 2D simulation was conducted using Exa Powerflow. A 3D model was imported into Powercase, but the simulated domain was at $Z=0\text{m}$, that is a 2D simulation using a 2.5D model, as the model is simple an extruded rounded rectangle, as visible in [Figure 2](#) and [Figure 3](#), and hence no model thickness was simulated. The advantage of using a 2D model is the more readily achievable analysis of drag and side-force variation due to inlet frequency as it avoids miscellaneous flow complexities that 3D models can create (especially those effects caused by wake vortex variation which can be very geometry specific). As such this paper aims to determine whether, generically, (i.e. not simply due to small detail geometry unique to one range or class of vehicle) whether the variation of airflow frequency affects vehicle drag and side-force, and hence the use of the simplified 2D model is of real value. One aspect of the tests was to simulate the experiment undertaken by Ryan [9], where a defined gust model (found from measuring real-world wind data) was translated over an idealised model (developed by Docton [8], [Figure 1](#) and [Figure 2](#)), this model being the basis of all the tests undertaken in this paper. [Figure 1](#) and [Figure 2](#) illustrate the computational domain and the 11 nested regions of mesh refinement. The cell resolution adjacent to the model in the full scale simulations was 2.0mm, as used in [7]. Periodic walls were used in $\pm Y$, with a velocity inlet and characteristic static pressure outlet defined. The test domain had 10 vehicle lengths up and 15 downstream of the model (i.e. 26 vehicle domain length) and 10 either side (so 21 vehicle domain width), based upon [10]. Powerflow is a time-resolved solver and the simulation time step used was $1.05 \times 10^{-5}\text{s}$.

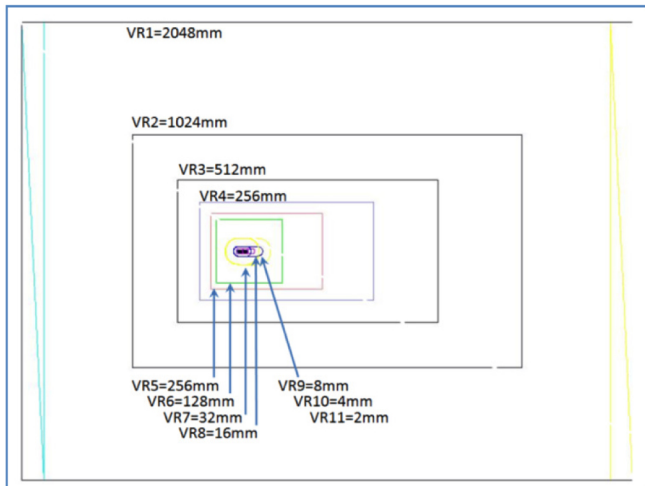


Figure 1. Powerflow case domain; note the range of variable resolution regions

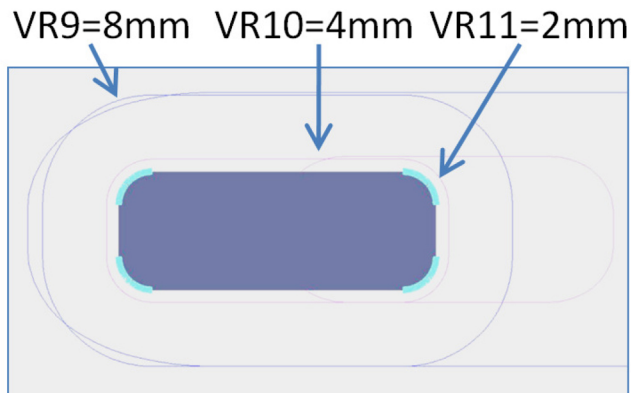


Figure 2. Powerflow domain with multiple VR regions and the Docton model

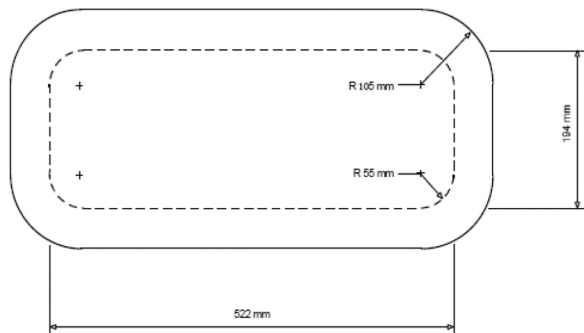


Figure 3. Docton model (1/8th scale) (from [18])

STEADY YAW ANALYSIS

A set of simulations was conducted with the full-sized Docton model set at a range of steady yaw angles from 0° to 10° in 2° increments. For all simulations presented here the axial component of inlet velocity was constant (30 ms⁻¹ for

the full size cases) and an additional crosswind component was introduced to create yaw. This means that the total resultant velocity is larger for higher yaw angles. This better mimics what is experienced on road than the common wind tunnel practise of running at constant velocity and yawing the vehicle due to the energy variation occurring with angle (i.e. namely the increased gust energy that is attributed with a gust flow angle change). It is also of value to fix the X-velocity as this ensures that the yawed flow is translated (or marched) over the model at a constant distance per time-step, reducing shear in the flow. Non-dimensional coefficients are based on the axial (e.g.: nominal driving velocity) rather than the total resultant velocity. Figure 4 illustrates the variation of drag coefficient with yaw angle while Figure 5 illustrates the corresponding variation of side force coefficient. The linear variation of side force with yaw angle is compared with the idealised “lift” slope predicted by potential flow theory. The projected frontal area for the coefficient calculations was kept the same for all yaw angles.

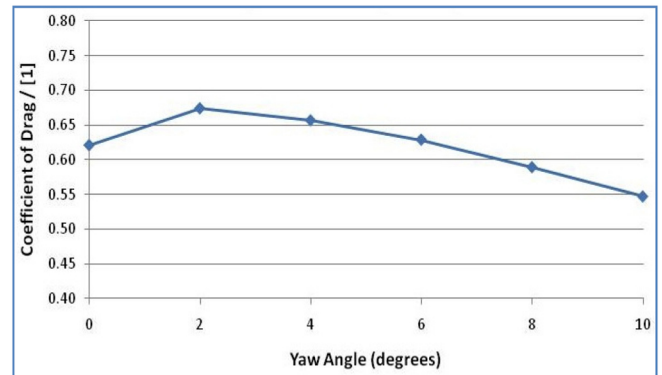


Figure 4. C_D with yaw angle for steady-state cases

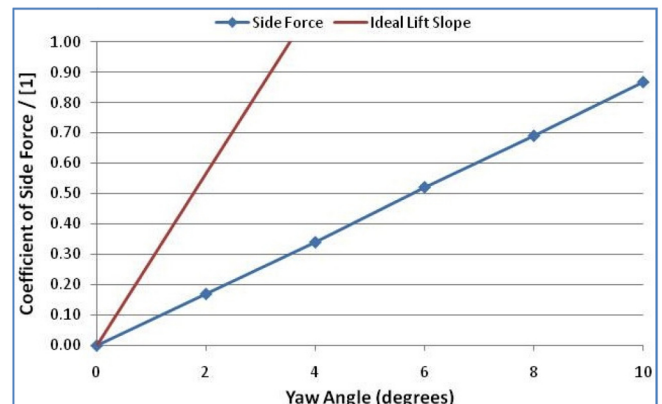


Figure 5. Coefficient of side-force with yaw angle for steady-state cases (ideal is $2\pi\alpha(L/W)$)

TRANSIENT EXTREME (27°) GUST

For validation of the expected flow characteristics and drag coefficient, Ryan's gust configuration [9], given in Figure 6, was used over the scaled Docton model [8] as in Figure 1. The Docton model represents a 1/8th scale model, that is around 15% size of a road vehicle, and the test was conducted to assess how the test model configuration replicated the force and transient response of the model in comparison to test data. Docton [8] had used this model in a crosswind wind-tunnel simulation at Durham with experimental drag results available in a time trace against gust time. The model configuration was essentially the same for this case and the other cases presented except that this one case was run at the reduced scale (and hence Reynolds number) used by Ryan [9] whereas the harmonic cases run later were at "full scale" in terms of model dimensions and Reynolds number. All of the important parameters (e.g.: mesh sizes) were scaled with the model scale.

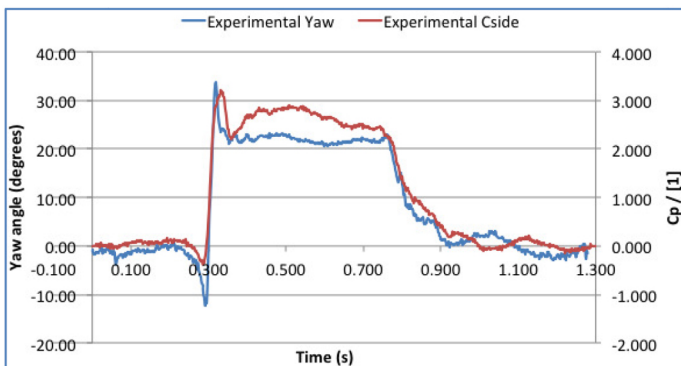


Figure 6. Experimental yaw and C_{SIDE} - [9]

Figure 6 illustrates Ryan's experimentally measured (empty test section) gust curve and his corresponding side force coefficient. Figure 7 presents the simulated yaw curve and force coefficients. It is evident that the model experiences a large side-force with a wide variation during the relatively steady gust, which would relate to a notable stability degradation. The two dimensional geometry exhibits vortex shedding and the results have been plotted with this spectral component removed for clarity in Figure 7. Vortex shedding removal was undertaken via Fourier Transform and then a transfer function suppressing frequencies above 30Hz, which was intuitively necessary as the higher frequency components made interpreting the main result, visually, much more challenging. The simulated result shows the same transient overshoot as the experimental measurement but it is clear that the overshoot is greater in the simulated case. Also, the simulation does seem to show slower transients than observed experimentally. These differences could easily be attributable to the fact that the rear geometry was of low aspect ratio (span/width) with endplates to encourage two-dimensional flow, whereas the simulated geometry is purely two-

dimensional. It could be argued that high aspect ratio, two-dimensional geometries tend to exhibit more extreme responses since stronger vortex shedding exists in 2D and the fact that flow cannot pass over the top of the model. Figure 7 does illustrate a lag between the CFD case and the experimental test. Though no exact cause for this was established, certainly the filtering of the 30Hz+ frequencies did remove noise elements that occurred in the initial side-force increase, and the CFD simulation may not accurately model this, effectively instantaneous, transient frequency. However, the harmonic frequencies do not operate at such a sharp transient frequency, and additionally the harmonic gust continues throughout the case simulation, so this issue does not undermine the conclusions given in the later cases.

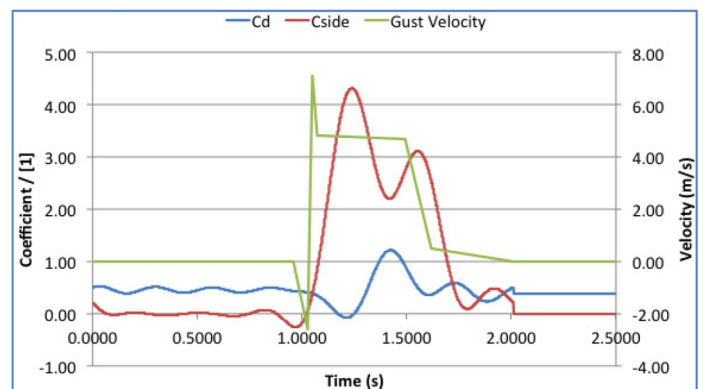


Figure 7. Simulated gust characteristic curve and resultant coefficients

HARMONIC INLET TESTS

A series of harmonic test cases were modelled using a full size version of Docton's 1/8th scale model, as in Figure 1. Inlet turbulence was at 1% intensity at 1m turbulence length scale, with V_X fixed at 30 m/s and V_Y varied as the inlet yaw velocity, with the default yaw angle peak being $\pm 6^\circ$ varying as a sinusoidal wave.

Tests were conducted at frequencies of 0.03, 0.15, 0.33, 1.75, 3.5, 7.0 and 10.0 Hz, which were selected in order to ensure capture of the critical reduced frequency threshold. All results are presented in reduced frequency based upon vehicle length.

In order to determine a steady equivalent drag coefficient (i.e. zero frequency point) the values from the "steady state" simulations were summed together in proportion to the area under the sine curve (i.e. basic numerical integration) that they occupied for a 6° sine wave. This gave a steady value (plotted as 0.01 reduced frequency on all the graphs for simplicity of comparison) of $C_D=0.62$. Similarly, the drag coefficient standard deviation would be 0.12 and the standard

deviation of side-force coefficient would be 1.46, under quasi-steady conditions.

The major constraints determining the simulation parameters for each configuration were: a fixed resolution for all cases, which fixes the physical time per time step, the number of ‘flush-throughs’ (labelled FTS, that is the number of times flow at the free stream velocity would replace all the fluid within the computational domain), the number of periods that will be simulated and the physical processing time for each case. This resulted in cases with between 1 and 8 million time-steps. The mesh was fixed for all cases, regardless of peak velocity magnitude as variance in mesh resolution was found to be significant in the variation of results, and the mesh refinement level used was determine, through a resolution study, to offer a ‘close to ideal’ results whilst using realistic levels of computing resources. In order to maintain a consistent number of measurements per period for the wide range of inlet frequencies, the following parameters were setup, as in [Table 1](#). For low frequency yaw fluctuations the physical time simulated is dictated by a requirement to simulate multiple yaw fluctuation periods while for high frequency yaw fluctuations the physical time simulated is dictated by a requirement for multiple flush throughs. Simulation time is given as ‘physical time’ since the number of time-steps varied between cases, but the physical time per time-step remained fixed for all cases, around 1×10^{-5} s per time-step. All cases were run using 4-cores per simulation, taking between 6-hours to 2-days for processing time, using Durham University's High Performance Computing ‘Hamilton’ cluster. The Logs/period refers to the measurement resolution, being defined as how many readings were taken for each foil oscillation period (and as such, it should be noted that the number of time-steps per log was varied between frequencies).

Table 1. Test setup matrix

Freq. (Hz)	Periods	FTS	Phys. Time (s)	Red. Freq.	Logs/period
0.03	2.5	50.2	82.7	0.03	634
0.33	11.5	21.1	34.7	0.29	443
1.75	60.7	21.1	34.7	1.53	136
3.50	44.2	7.7	12.6	3.06	136
7.00	44.2	3.8	6.3	6.12	136
10.0	63.1	3.8	6.3	8.75	127

The harmonic flow can be visualised as in [Figure 8](#) and [Figure 9](#), where the plots of a 1 Hz and 10 Hz wave have been plotted in scale with the model.

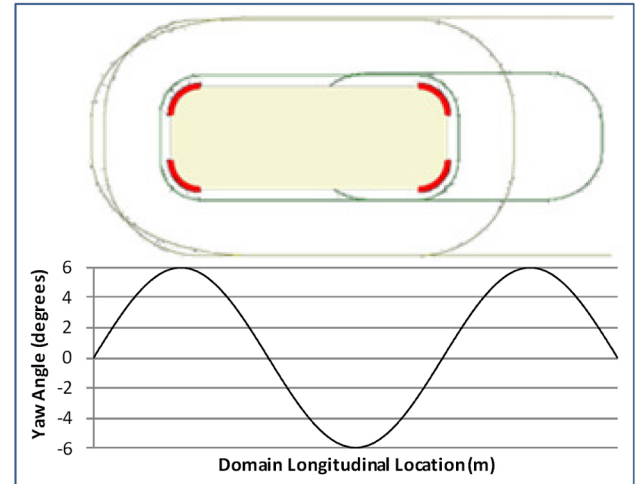


Figure 8. Yaw scale at $\omega R = 3.00$ (10 Hz)

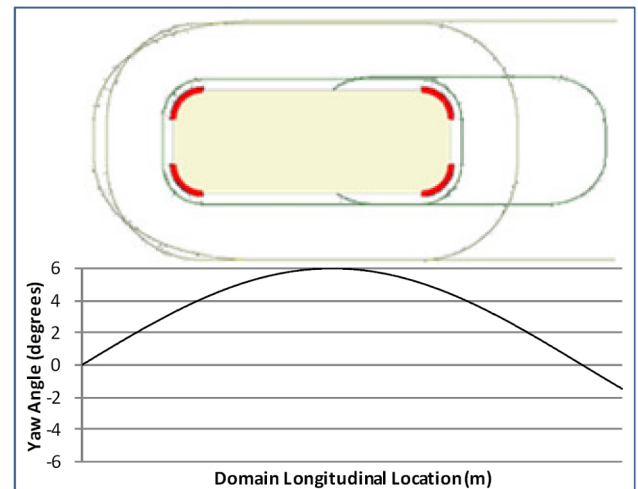


Figure 9. Yaw scale at $\omega R = 0.30$ (1 Hz)

Investigations are also included varying Reynolds number and exploring non-linearity in the vehicle's response to yaw fluctuations of different magnitudes and comprising multiple superimposed frequencies. Further geometry cases were evaluated for varying corner radii and vehicle width. The geometries tested were relatively extreme variations of the Docton model; the widths were the 132.3 and 284mm following Sims-Williams [10]. The range of studies conducted were:

- Yaw angles of 0, 2, 4, 6, 8 and 10-degrees for a steady 30ms^{-1} inlet using the full-sized model.
- Frequency analysis at 0.03, 0.15, 0.33, 1.75, 3.5, 7 and 10Hz for 6-degree yaw.
- A viscosity analysis running the setup at 0.03, 1.75, 3.50 and 10Hz for standard, atmospheric viscosity $\times 4$ and standard viscosity/10000.

- 30mm, 55mm and 80mm corner radii at 0.03, 1.75, 3.50 and 10Hz.
- 132.3, 194 and 284 mm widths (i.e. aspect ratio variance) at 0.03, 1.75, 3.50 and 10Hz.
- 3, 6, 12 and 20° peak yaw angle tests at 0.03, 1.75, 3.50 and 10Hz.
- Superimposed frequencies of 3.5+0.33Hz and 3.5+10Hz.
- All drag and side-force coefficients were determined using the 3D x-axis project frontal area, determined through the CFD package and adjusted for yawed models. This is consistent with Powerflow manual advice for 2D simulations of a 2.5D or 3D model.

FREQUENCY RANGE

A range of frequencies was tested, from $\omega_R = 0.03$ to $\omega_R = 8.8$ (0.03Hz to 10Hz) for 6° peak yaw. [Figure 10](#) illustrates the variation of drag coefficient over two periods for each of these cases. All the cases include a fluctuation at approximately 3.5 Hz ($\omega_R \sim 3$ based on length, Strouhal Number 0.27 based on width); the physical time bases for the different cases varies by more than two orders of magnitude and so in some cases the shedding is at a relatively much higher frequency and in others it is at a lower frequency than the yaw fluctuations. In [Figure 10](#) and [Figure 11](#) the traces have been reset such that the yaw angle plotted corresponds with the angle at the front of the car, and as such any phase shift visible between the frequency traces is a true phase difference experienced by the model. For the $\omega_R = 0.03$ and 0.33 cases the fluctuations due to vortex shedding have been filtered from the output traces for clarity. Note that the drag varies at twice the driving frequency of the yaw sine wave, since positive and negative yaw each have the same effect on drag.

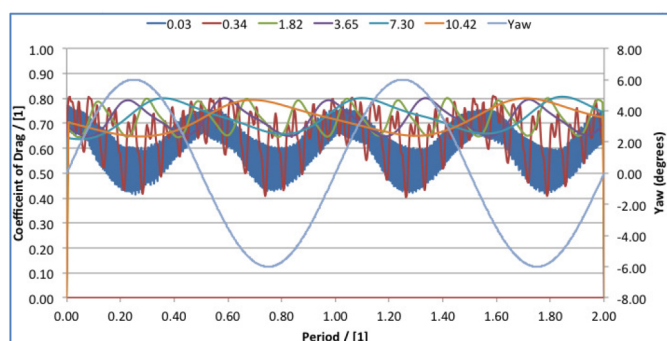


Figure 10. Period plot of C_D for 2-periods of developed flow

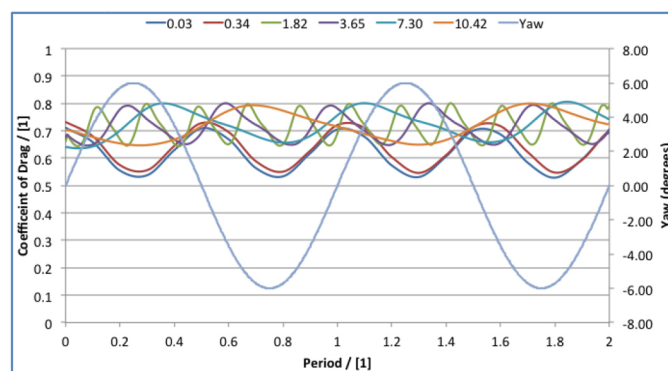


Figure 11. Filtered results of C_D with period number

[Figure 12](#) presents the corresponding variation in side force coefficient, which naturally averages to zero. It is visible that the side-force varies greatly over the gust cycle. Note that as expected the side-force oscillates at the same frequency as the driving frequency.

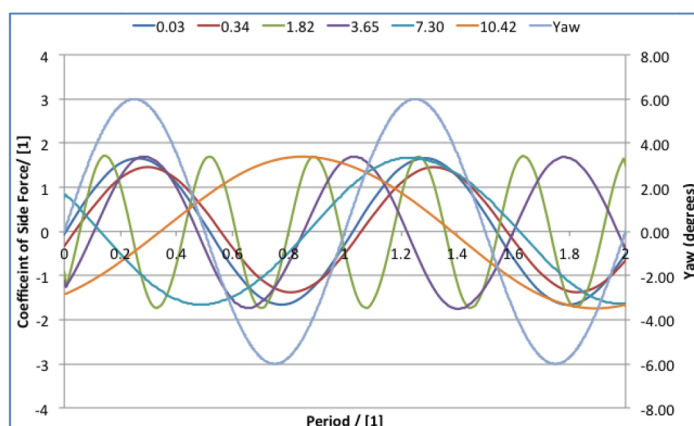


Figure 12. Filtered coefficient of side-force with period

[Figure 13](#) illustrates the variation of average drag coefficient with reduced frequency across this set of the simulations (using the $\omega_R = 0.03$ case as a baseline). Averages and standard deviations were everywhere calculated over an integer number of periods, which is essential to avoid biasing the results. The point plotted at a reduced frequency of 0.01 is the true quasi-steady case derived from simulations at steady yaw angles. It is evident that a prominent drag increase ($\Delta C_D = 0.10$) occurs between reduced frequencies of 0.3 and 1.5. Fundamental work in aeronautics (e.g.: as discussed by He [12] and others) has indicated that we would expect reduced frequencies below $\omega_R = 0.1$ to be quasi-steady but for unsteady effect to become important for reduced frequencies somewhere between 0.1 and 1.0, the result of [Figure 13](#) fits this theory well. The drag coefficient effect between $\omega_R = 0.3$ and 1.5 observed here would correlate to a full-scale frequency of 0.33-1.75 Hz, equivalent to length scales of 17

m - 90 m or 4 to 20 vehicle lengths. This result is in keeping with the observations of Docton [18] that the flow around a model subjected to a step change in yaw angle requires about 7 vehicle lengths to reach a steady state. This figure also shows that for reduced frequencies above 1.5 further changes in drag coefficient are small, indicating that for this geometry at least shorter length scales do not bring any different effects. It should be noted in Figure 13 that normalised means that all results were rebased from the lowest drag value, and that at each frequency location the data point is evaluated as the mean over the full unsteady simulation time.

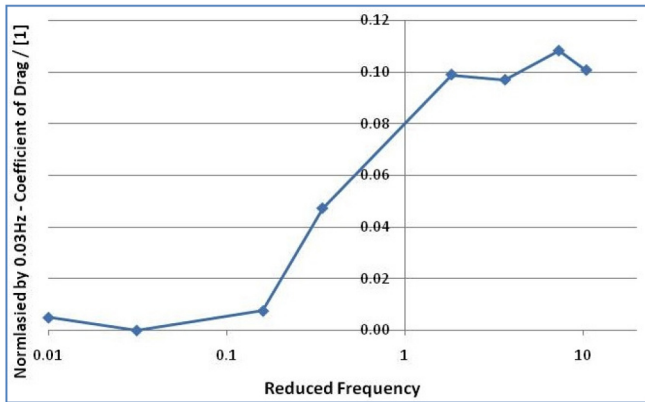


Figure 13. Variation of normalised average C_D with reduced frequency

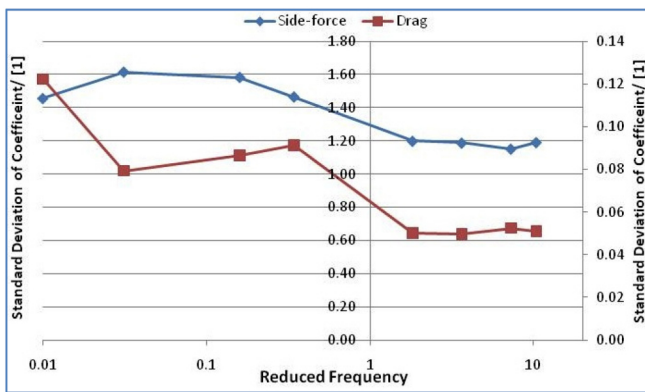


Figure 14. Drag and side-force deviation with reduced frequency (LHS scale for drag, RHS scale for side-force)

Figure 14 illustrates the magnitude of the time variation of side-force as well as drag and demonstrates an approximately similar critical frequency range. As expected, the magnitude of the force fluctuation decreases with increasing frequency. This figure is akin to an aerodynamic admittance. The results have been given in side-force coefficient rather than yawing moment as the yawing moment showed more extreme behaviour than the side-force coefficient because the gust front scans along the length of the model, which has a more dramatic transient effect on yawing moment than side-force.

By quoting results in side-force, this offers a more direct comparison to the drag coefficient, which were both, averaged over the same periods.

REYNOLDS NUMBER VARIATION

Reynolds number effects were investigated by changing the fluid viscosity. This assessment was to see to see if the viscosity was important to the non-steady effects, or if the effects were principally inviscid, and simply that the highest Reynolds number was very high (i.e.: towards inviscid). As a moving transition point is just one effect of changing viscosity, (and as Powerflow cannot model boundary layer transition) it was of interest to see whether other effects would be noted. Increasing the viscosity by a factor of 4 gave a low Reynolds number flow perhaps corresponding to a small scale model test, whilst reducing the viscosity by four orders of magnitude resulted in an almost inviscid flow. This makes it possible to identify whether the non-quasi steady effects observed above are viscous or inviscid effects. Figure 15 shows the change of the averaged drag coefficient with reduced frequency at the three different Reynolds numbers. Note that the scale of the figure has to be relatively large in order to accommodate the large reduction in steady state drag in the inviscid case. While viscosity obviously has a significant effect on the total drag, the model sensitivity to yaw fluctuations at different frequencies is broadly similar in magnitude and in terms of critical reduced frequency, over a Reynolds number variation of several orders of magnitude around that of interest for road vehicles. It can be concluded that the non quasi-steady effects (that is the effect of varying frequency as found earlier) occur regardless of viscosity. Figure 16 shows the reduction in side-force deviation with frequency and again this effect is not substantially altered by viscosity.

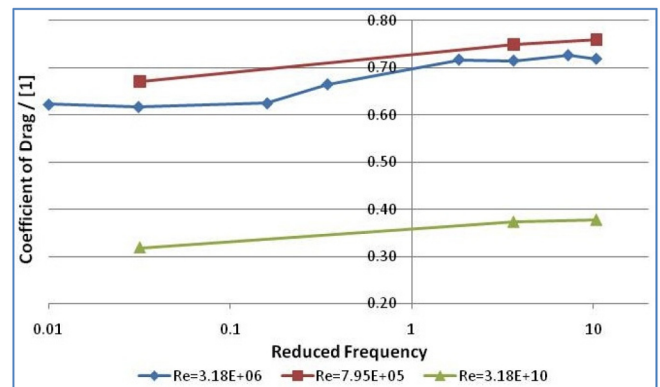


Figure 15. Normalised C_D (relative to lowest frequency in respective subset) with reduced frequency

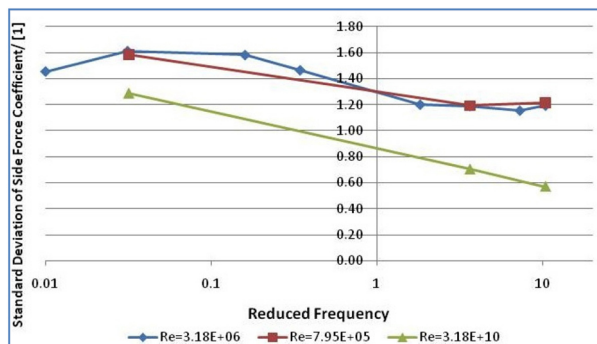


Figure 16. Side-force deviation with reduced frequency

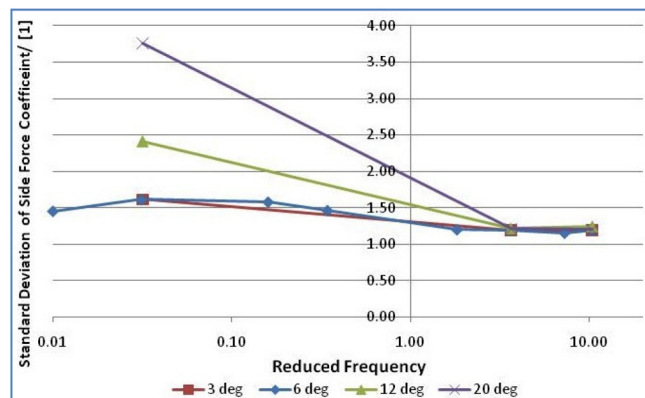


Figure 18. Side-force deviation with reduced frequency

YAW AMPLITUDE VARIATION

Figure 17 shows the change in drag coefficient with reduced frequency for a range of yaw amplitudes. This confirms that the variation in peak angle does not significantly affect the critical reduced frequency limit. Seemingly surprisingly, increasing yaw magnitude does not produce a corresponding change in average drag. This is in part because at all yaw angles the axial velocity component is the same. It is evident in Figure 18 that the side-force deviation at low frequencies is much more prominent than at higher frequencies, and that above the critical reduced frequency limit the side-force deviation becomes consistent over the peak-yaw angle range. It should be again noted that the resultant velocity is large at high peak yaw angles, hence the increased side-force coefficients, not simply because the yaw angle has been increased but also due to the increased total resultant velocity. Nevertheless, Figure 18 illustrates that the change in transient force at increased frequency is not linear with the forcing function. The attractive concept of an aerodynamic admittance or transfer function between forcing function and vehicle response essentially assumes a linear response to forcing function and so could not correctly model this case.

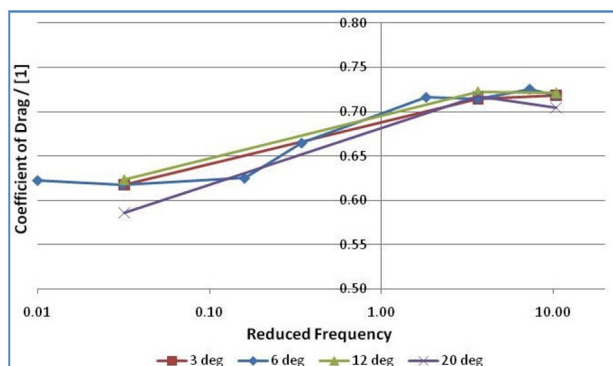


Figure 17. C_D versus reduced frequency for a variation in peak yaw angle

SUPERPOSITION OF MULTIPLE FREQUENCIES

Again, attractive concepts such as aerodynamic admittance rely on a linear response and this would mean that the incremental impact of a forcing function at a particular frequency would be the same as the impact of that forcing function in isolation. This hypothesis was tested by superimposing two independent yaw fluctuations at different frequencies. The superimposed cases are where a 3.5 Hz ($\omega_R = 3$) case, seen as a frequency very close to the quasi-steady limit, is added to a 0.03 Hz ($\omega_R = 0.03$) in one case and a 10 Hz ($\omega_R = 9$) frequency in the second case. In comparing the effect of adding a lower frequency to the 3.5Hz ($\omega_R = 3$) case and similarly a higher frequency to the 3.5 Hz case it is possible to test linearity and if multiple frequencies impact the critical frequency limit. It is visible in Figure 19 that the resultant drag coefficient of a case is based upon the frequency that creates the greatest drag coefficient. For example, the C_D of 3.5 Hz ($\omega_R = 3$) case is around 0.72, whereas the C_D at 0.03 Hz ($\omega_R = 0.03$) is around 0.62. However, superimposing the two in equal ratios (both at full energy, that being 6° for both sine waves) has resulted in the actual C_D being that of the 3.5Hz case, not the lower C_D from the 0.03 Hz case or the sum of the two separate effects. This effect is repeated with a 10 Hz superposition inlet. This leads to the same conclusion as the yaw magnitude test, that the model aerodynamic response is non-linear. It is also suggested that the resultant C_D experience by an idealised geometry will be that of the greater drag from the higher frequency component, which will namely be the frequencies above the quasi-steady limit as these frequencies have been show to generate the highest drag coefficients.

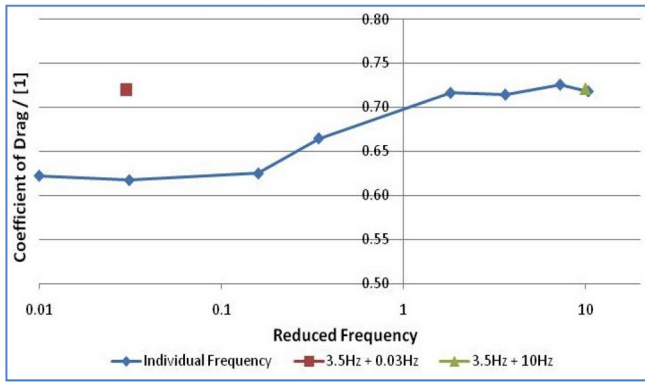


Figure 19. C_D with reduced frequency for varying superposition

Figure 20 again correlates with earlier graphs showing a 25% reduction in C_D variation for increased inlet frequency. Additionally it is of interest that as the drag force corresponds to the highest drag coefficient from the superimposed inlet frequency with the highest individual drag coefficient, the side-force deviation result relates to the lowest individual component. As such though the drag will be greater, the range will be less, which reduces the peak intensity requirement for simulation.

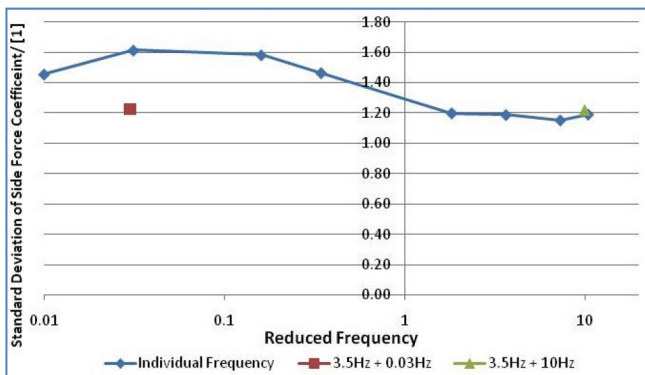


Figure 20. Deviation of side-force with reduced frequency for varying superposition

Figure 21 and Figure 22 illustrate the point further. It can be seen that the effect of having two frequencies is non-summative, and the result is much more comparable to running either at double the peak yaw angle or the drag of the highest individual frequency drag result. This is also visible in the side-force coefficient plot where the superposition result is much like running the case at double the peak yaw angle or equally the resultant side-force from the individual frequency that has the lowest side-force deviation in its own right.

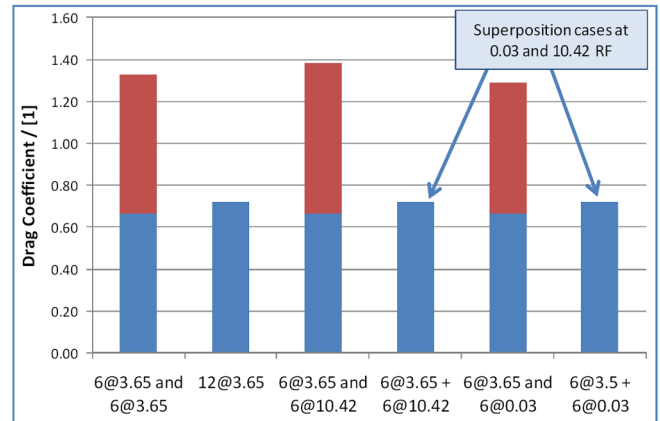


Figure 21. Comparison of C_D for similar inlet setups

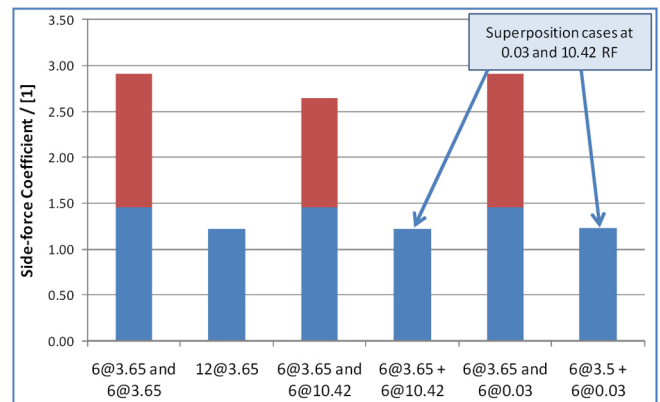


Figure 22. Comparison of side-force coefficients for similar inlet setups

EFFECTS OF MODEL WIDTH AND CORNER RADII

The normalised plots of drag coefficient in Figure 23 and Figure 24 show that the critical reduced frequency limit is maintained but that the effect of the frequency increase on drag coefficient is affected by the model's geometry. Figure 23 displays that as a model's width is reduced (i.e. the model is less bluff) that the effect of increase in frequency becomes more prominent. It is also evident that after the critical reduced frequency is exceeded the drag coefficient plateaus. Figure 24 shows that the reduction in corner radius (i.e. sharper corners) causes the effect of frequency increase to become more significant.

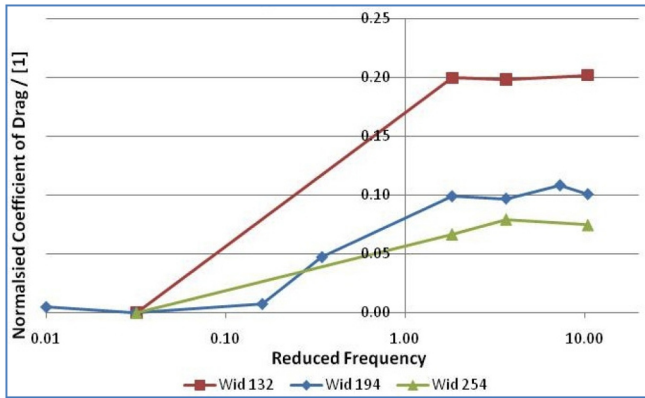


Figure 23. C_D with reduced frequency for varying width

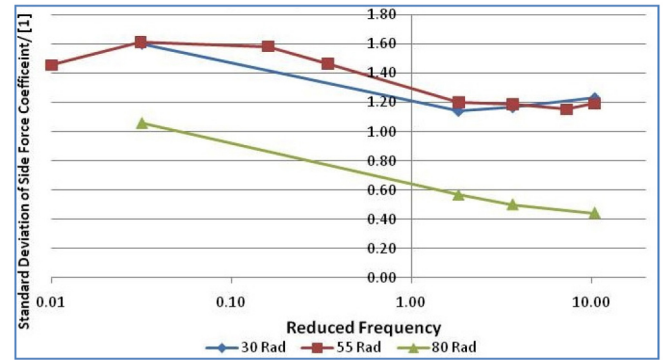


Figure 26. Deviation of side-force with reduced frequency for varying corner radii

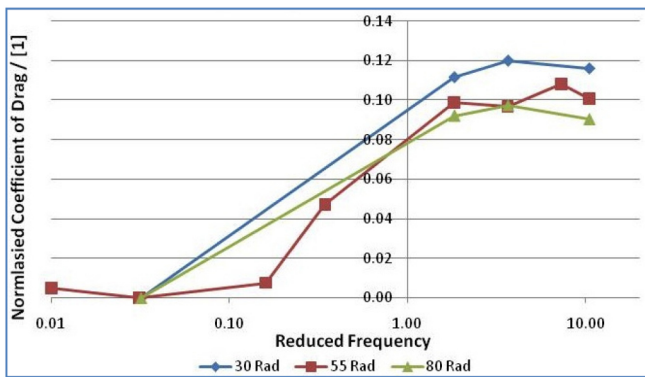


Figure 24. Normalised C_D with reduced frequency for varying corner radii

Figure 25 and Figure 26 detail the reduction in side-force deviation with increase in frequency, as seen in earlier results. In conclusion, models that are long in aspect ratio, and with sharp corners, experience greater drag increase with frequency than wider models with more rounded corners.

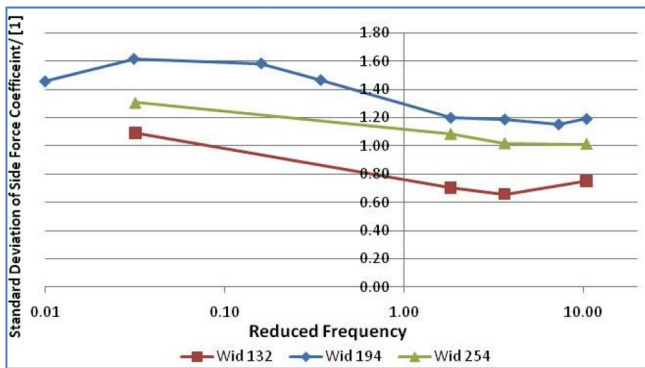


Figure 25. Deviation of side-force with reduced frequency for varying width

SUPERPOSITION OF CONSTANT YAW OFFSET

The results given in this paper so far have all been with a sine inlet function with a zero yaw mean flow. In practise the average yaw angle seen on the road is a few degrees and turbulence fluctuations will be superimposed on that. All of the CFD tests described were also fully evaluated with a mean yaw angle of 3° and superimposed sine fluctuation. In this case the amplitude of the sine wave was 3° rather than 6° . An example of the results for this case is given in Figure 27. This confirmed that the critical reduced frequency threshold was similar, albeit slightly more abrupt than for the zero mean yaw cases, being just above $\omega_R = 0.03$. This alternative condition also produced similar conclusions with respect to the impact of viscosity and model geometry.

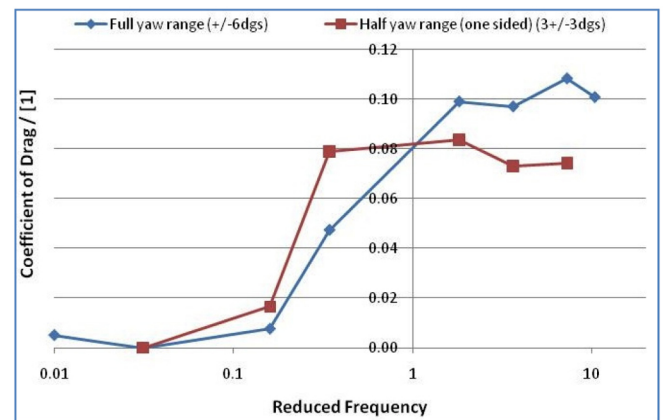


Figure 27. Effect on Drag With and Without Yaw Offset

CONCLUSIONS

It was found that for most aspects, and especially for time-averaged drag, the flow could be treated as quasi-steady for reduced frequencies below 0.3, in line with expectations. The most significant changes were observed in a critical reduced

frequency range between $\omega_R = 0.3$ and $\omega_R = 1.5$. This corresponds to scales of 4-20 vehicle lengths, or 17 m - 90 m or periods of 0.6 to 3s or frequencies of 0.33 Hz to 1.75 Hz (for a full scale vehicle at 30 m/s). Frequencies larger than this range will have significant effects, but in this case the effects showed little frequency sensitivity once above the critical range.

A real vehicle will have physical features (e.g.: wing mirrors) on scales smaller than that of the entire vehicle. The critical reduced frequency range for these features will therefore correspond to smaller physical scales and so will bring importance to these scales smaller (but not larger) than the 4-20 vehicle length scale.

The effect of the yaw variation (at constant axial velocity) was to increase time-average drag coefficient and the variation of drag coefficient and side force coefficient. These effects increased with frequency through the critical range detailed above and then saturated, with higher frequencies producing the same effect as frequencies just above the critical range.

The dynamic effects were largely independent of Reynolds number, including for near-inviscid conditions. This indicates that the sources of non-quasi-steady response are not viscous in origin.

Increasing yaw amplitude or combining multiple frequency components did not have a summative impact on the time averaged or time varying drag and side force. Care therefore needs to be taken in trying to describe vehicle response to transient conditions using linear concepts such as transfer functions or admittance functions. When superimposing different frequencies the resulting average drag was close to that of the individual frequency component with the highest isolated impact on drag. The side-force deviation was consistent also with the individual frequency that had the lowest deviation in the frequency range.

It was found that narrow bodies with sharper corners caused a greater time-averaged drag coefficient change with frequency compared with rounder or wider bodies. As a general conclusion, this paper found that moving from longer to shorter length scales (i.e. lower to higher inlet frequencies), especially in the region where the length scales are in the order of the vehicle length, will have a notable effect on vehicle drag and side-force. It should be re-iterated that these conclusions are based upon an ideal 2D model, which removes many flow complexities associated both with small-sized component geometries and 3D viscous flow effects. However, the results, equally because of this simplification, therefore are valid in developing the understanding of how a rounded bluff body's (which typically all vehicles are) performance will vary with single-component inlet frequency

variation, and hence the conclusions could be expanded to tri-axis inlet frequency variation for 3D models.

REFERENCES

1. Cooper, K.R. and Watkins, S., "The Unsteady Wind Environment of Road Vehicles, Part One: A Review of the On-road Turbulent Wind Environment," SAE Technical Paper [2007-01-1236](#), 2007, doi:[10.4271/2007-01-1236](#).
2. Watkins, S. and Cooper, K.R., "The Unsteady Wind Environment of Road Vehicles, Part Two: Effects on Vehicle Development and Simulation of Turbulence," SAE Technical Paper [2007-01-1237](#), 2007, doi:[10.4271/2007-01-1237](#).
3. Sims-Williams, D.B., "Cross-Winds and Transients: Reality, Simulation and Effects," Keynote Address at SAE World Congress, Detroit, 2010.
4. Cogotti, A., "Generation of a Controlled Level of Turbulence in the Pininfarina Wind Tunnel for the Measurement of Unsteady Aerodynamics and Aeroacoustics," SAE Technical Paper [2003-01-0430](#), 2003, doi:[10.4271/2003-01-0430](#).
5. Schoeck, D., Widdecke, N., and Wiedemann, J., *Aerodynamic Response of a Vehicle Model to Turbulent Wind*, in *7th FKFS Conference, Prog. Vehicle Aerodynamics and Thermal Manag.* 2009: Stuttgart.
6. Tsubokura, M., Takahashi, K., Matsuuki, T., Nakashima, T. et al., "HPC-LES for Unsteady Aerodynamics of a Heavy Duty Truck in Wind Gust - 1st Report: Validation and Unsteady Flow Structures," SAE Technical Paper [2010-01-1010](#), 2010, doi:[10.4271/2010-01-1010](#).
7. Gaylard, A., Beckett, M., Gargoloff, J.I., and Duncan, B.D., "CFD-based Modelling of Flow Conditions Capable of Inducing Hood Flutter, SAE Technical Paper [2010-01-1011](#), 2010, doi:[10.4271/2010-01-1011](#).
8. Docton, M., *The Simulation of Transient crosswinds on Passenger Vehicles*. Durham University PhD Thesis, 1996.
9. Ryan, A., *The Simulation of Transient Cross-Wind Gusts and Their Aerodynamic Influence on Passenger Cars*. 2000, Durham University.
10. Sims-Williams, D.B., *Self-Excited aerodynamic unsteadiness associated with passenger cars*. Durham University PhD Thesis, 2001.
11. Theissen, P., *Unsteady Phenomena in Vehicle Aerodynamics under Time-Dependent Flow Conditions*. University Thesis, 2010.
12. He, L., *Analysis of Quasi-Steady Limit for Idealised Models*. PhD Thesis, Durham Univeristy, 1996.
13. Wordley, S. and Saunders, J., "On-road Turbulence: Part 2," *SAE Int. J. Passeng. Cars - Mech. Syst.* **2**(1):111-137, 2009, doi:[10.4271/2009-01-0002](#).

14. Schröck, *Aerodynamic Response of a Vehicle Model to Turbulent Wind*. FKFS, 2009.
15. Newnham, P., Passmore, M., and Baxendale, A., "The Effect of Raised Freestream Turbulence on the Flow Around Leading Edge Radii," SAE Technical Paper [2008-01-0473](#), 2008, doi:[10.4271/2008-01-0473](#).
16. Newnham, *On the optimization of road vehicle leading edge radius in varying levels of free stream turbulence*. 1995.
17. Peinke, *Atmospheric Wind Field Conditions Generated by Active Grids*. 2010.
18. Docton, M., *The Simulation of Transient Cross Winds on Passenger Vehicles*, in *School of Engineering*. 1996, Durham University.

CONTACT INFORMATION

Oliver Mankowski
School of Engineering
South Road
Durham
DH1 3LE
o.a.mankowski@dur.ac.uk

ACKNOWLEDGMENTS

The authors are grateful for the support of Jaguar Land Rover and Exa associated with the use of the Powerflow software suite. Joaquin Gargoloff at Exa provided particular assistance. The authors are also grateful to Anthony Ryan for providing the experimental data used for validation.

DEFINITIONS/ABBREVIATIONS

TGS

Turbulence Generation System

ABL

Atmospheric Boundary Layer

The Engineering Meetings Board has approved this paper for publication. It has successfully completed SAE's peer review process under the supervision of the session organizer. This process requires a minimum of three (3) reviews by industry experts.

All rights reserved. No part of this publication may be reproduced, stored in a retrieval system, or transmitted, in any form or by any means, electronic, mechanical, photocopying, recording, or otherwise, without the prior written permission of SAE.

ISSN 0148-7191

Positions and opinions advanced in this paper are those of the author(s) and not necessarily those of SAE. The author is solely responsible for the content of the paper.

SAE Customer Service:

Tel: 877-606-7323 (inside USA and Canada)

Tel: 724-776-4970 (outside USA)

Fax: 724-776-0790

Email: CustomerService@sae.org

SAE Web Address: <http://www.sae.org>

Printed in USA